I/σI *vs* {Rmerg, Rmeas, Rpim, CC1/2} for Crystal Diffraction Data Quality Evaluation

Zheng-Qing Fu[1,2,*], Brian V. Geisbrecht[3], Samuel Bouyain[4], Fred Dyda[5], John Chrzas[1,2], Palani Kandavelu[1,2], Darcie J. Miller[6] and Bi-Cheng Wang[1,2]

[1]SER-CAT, Advanced Photon Source
Argonne National Laboratory
Argonne, IL 60439, USA

[2]Department of Biochemistry & Molecular Biology
University of Georgia
Athens, GA 30602, USA

[3]Department of Biochemistry & Molecular Biophysics
Kansas State University
Manhattan, KS 66506 USA

[4]Division of Biological and Biomedical Systems
School of Science and Engineering
University of Missouri – Kansas City
Kansas City, MO 64110, USA

[5]Laboratory of Molecular Biology
The National Institute of Diabetes and Digestive and Kidney Diseases
Bethesda, MD 20892-0560. USA

[6]Department of Structural Biology
St. Jude Children's Research Hospital
Memphis, TN 38105

*Corresponding Author

Abstract

X-ray crystal diffraction has provided atomic-level structural information on biological macromolecules. Data quality determines the reliability of structural models. In most cases, multiple data sets are available from different crystals and/or collected with different experimental settings. Reliable metrics are critical to rank and select the data set with the highest quality. Many measures have been created or modified for data quality evaluation. However, some are duplicate

in functionality, and some are likely misused due to misunderstanding, which causes confusion or problems, especially at synchrotron beamlines where experiments proceed quickly. In this work, the capability, significance, effectiveness, and correlations of these measures are studied through both theoretical analysis and experimental data to clarify confusion and misuses, and thus identify the most reliable measures for evaluating data quality from different aspects.

Introduction

Macromolecular structures have provided a powerful tool for understanding biological function and have played a pivotal role in design of pharmaceuticals. X-ray diffraction, with a century-long and continuous development, has become a primary method to solve 3D structures of macromolecules in terms of number of structures, apparent resolution, and quality. Without the hurdle set by crystallization, Cryo-EM (Dubochet et al., 2018; Frank, 2009; Henderson et al., 1990; Cheng et al., 2015) has recently risen to be a significant force in solving macro molecular structures, especially for those with multiple-chain ensembles. Furthermore, owing to advances in genomics, detection technology, data analysis software, and more recently the advent of AI-based model prediction, the PDB (Berman et al., 2000; Berman et al., 2003, Burley et al., 2023) database has grown dramatically to provide homologous models to be used in solving most new structures by X-ray diffraction or Cryo-EM. As in any experiment, an effective and reliable metric is critical to evaluate and select the best X-ray diffraction data set for structural solution. Historically, $I/\sigma I$ and/or Rmerg (a.k.a Rsym) were used to evaluate data quality. Rmerg has been shown to have drawbacks due to its dependency on multiplicity. To improve upon this limitation, Rmeas (Diederichs et al., 1997) and Rpim (Weiss et al., 1997) were introduced by accounting for multiplicity into the equation for Rmerg. Traditionally, resolution cutoffs are selected by $I/\sigma I \geq 2.0$

and/or {Rmerg, Rmeas, Rpim}≤40%, 50%, 60% etc. in the highest resolution shell. More recent studies showed that this may be too conservative as it could exclude weak but still useful reflections within the higher resolution shells; this resulted in the introduction of the index CC1/2 (Karplus et al., 2012; Karplus et al., 2015) to try to address the issue. However, CC1/2 does not have a clearly meaningful threshold that is generally applicable. Different values (such as 0.4, 0.3, 0.2, 0.1 etc.) have been suggested to select data and used as data processing programs' defaults, or defaults customized by users at different sites, which causes confusion in practice during data collection and processing. Although these different measures have been developed and used to evaluate and select data from X-ray crystal diffraction experiments, what is the best and how to select the best data set remains debatable. This situation is magnified when using synchrotron beamlines, where experiments proceed at a fast pace. In this work, their meaning, correlation, significance, and effectiveness are studied through both theoretical analysis and experimental data with various characteristics to clarify the confusion and any potential misuses, and thus to identify the most reliable measures for evaluating data quality from different aspects.

Methods

Some background knowledge is summarized here first for easier reading and for helping understand the subjects involved. Data from diffraction experiments are reduced to a set of unique reflections by minimizing differences among the equivalent reflections through target function (1) during data processing (Hamilton et al., 1965; Otwinowski et al., 1997; Kabsch, 2010; Leslie et al., 2007; Evans, 2011; Fu, 2005; Winter et al., 2018; Giacovazzo, 1992),

$$\psi = \sum_{k}^{\mathrm{Nc}} \sum_{i}^{\mathrm{Nr}} \sum_{j}^{\mathrm{Ne}} \left(\frac{\mathrm{S}(i,j,k)\mathrm{I}(i,j,k) - \langle \mathrm{I}(i) \rangle}{\sigma \mathrm{I}(i,j,k)} \right)^2 \qquad (1).$$

The discrepancy index associated with the minimization process can be calculated by

$$\mathrm{Rmerg} = \frac{\sum_k^{\mathrm{Nc}} \sum_i^{\mathrm{Nr}} \sum_j^{\mathrm{Ne}} |\mathrm{S}(i,j,k)\mathrm{I}(\mathrm{i,j,k}) - \langle I(i) \rangle|}{\sum_k^{\mathrm{Nc}} \sum_i^{\mathrm{Nr}} \sum_j^{\mathrm{Ne}} |\mathrm{S}(i,j,k)\mathrm{I}(\mathrm{i,j,k})|} \quad (2).$$

Here *j* runs through the equivalent reflections (denoted as including both repeated measurements of same reflection and those related by Laue group symmetry of the crystal, hereafter in this article for simplicity), *i* runs through the unique reflections, and *k* runs through the number of data sets if multiple data sets are involved. I(*i*,*j*,*k*), σI(*i*,*j*,*k*), are the observed intensity and estimated error, and S(*i*,*j*,*k*) are scaling factors. <I(*i*)> (denoted as I(*i*) for simplicity hereafter) and σI(*i*) are the merged intensity from equivalents and the estimated error or noise for each unique reflection **H**(*i*). The result of data processing is the reduced data set {**H**(*i*), I(*i*), σI(*i*) | *i*=1, N_r} consisting of the unique reflections up to a selected resolution (a.k.a. resolution cutoff). The number of unique reflections N_r is determined by the resolution cutoff selected.

As shown in equation (1), the fundamental of raw data reduction from a diffraction experiment is to minimize the differences among intensities of equivalent reflections. Rmerg, as the standard discrepancy index associated with the minimization, provides a measure of quality of the data set in terms of equivalency or internal consistency (Evans et al., 2013).

The second quality indicator of the reduced data set is the merged <I/σI> (denoted as I/σI hereafter for simplicity). I/σI is necessary as it provides quality evaluation from a different aspect, namely the signal-to-noise ratio (SNR as commonly denoted). SNR is fundamental to all experiments as it compares the level of a desired signal to the level of background noise.

The third fundamental quality indicator is the completeness (denoted as *Compl* hereafter for simplicity), because the electron density map (commonly calculated as a weighted 2Fo-Fc map during structure refinement) is Fourier transform of the reflections (Giacovazzo, 1992),

$$\rho(\boldsymbol{X}) = \frac{1}{V}\sum_{i}^{\mathrm{Nr}}\sum_{k}^{Ns}|2w\boldsymbol{F}o(i,k)| - |\boldsymbol{DF}c(i,k)| \cdot \exp\left[-2\pi i(\boldsymbol{H}(i,k)\cdot\boldsymbol{X} - \varphi\mathrm{c(i,k)})\right] \quad (3a),$$

$$\boldsymbol{F}c(i,k) = \frac{1}{V}\sum_{m}^{\mathrm{Nm}}\sum_{k}^{Ns} f(m,B)\cdot\exp\left[-2\pi i(\boldsymbol{H}(i,k)\cdot\boldsymbol{X}(k,m)\right] \quad (3b).$$

Here i runs through the unique reflections {**H**(i), I(i), | i=1, N_r}, and k runs through symmetry operations. φ_c(i,k) is the phase of reflection structure factor. $|Fo(i,k)| = \sqrt{I(i)}$. m runs through all atoms in the asymmetric unit. $f(\mathrm{m,B}) = \mathrm{f(m)}\cdot\exp\left(-\mathrm{B}\cdot\frac{\sin^2(\theta)}{\lambda^2}\right)$ with f(m) as the atomic form factor and θ the diffraction angle. B is the temperature factor that is evaluated during structure refinement (Afonine et al., 2012; Murshudov et al., 2011). **X**(k,m) are the coordinates of atom (k,m). **F**c(i,k) is the calculated structure factor using both coordinates and B factors of all atoms in the structure. In most diffraction experiments, not all reflections are measurable, leading to N_r being less than N_{rc} (the theoretically expected number of unique reflections to a given resolution). If some reflections are missing, it could affect the quality of the electron density map and, thus, the structure model built. The ratio N_r/N_{rc} directly measures the completeness of the reduced data set. In practice, 100% completeness is not required to calculate a tracible (or solvable) electron density map. But the lower it is, the less tracible the electron density would be. It is worth noting that missing wedge, anisotropy, or overloads can introduce systematic incompleteness and have different impacts than random incompleteness, which is not the subject of this study.

Theoretically, Rmerg, I/σI, and *Compl* are the fundamental measures needed to evaluate the quality of a reduced data set, which would, in turn, determine the quality of the structure. However, since I(i) and σI(i) are merged from equivalent reflections, the number *Ne* as shown in equation (1) will

affect I(i) and σI(i), leading to another measure 'multiplicity' (denoted as *Multi* hereafter) calculated as the average of *Ne*. Rmerg evaluated from equation (2) will be affected by *Multi*, such that the higher *Multi* the worse the Rmerg. As merging reduces the random noise, more measurements will typically lead to better quality of reduced data if no severe crystal decay occurred during the experiment. To compensate for this effect, Rmeas (Diederichs et al., 1997) was introduced by adding $\sqrt{Ne/(Ne-1)}$ to equation (2). Intended to indicate the precision of the measurements, another alternative, Rpim was defined with a different factor $\sqrt{1/(Ne-1)}$ (Weiss et al., 1997).

CC1/2 is an indicator more recently introduced for selecting resolution cutoff (Karplus et al., 2012; Karplus et al., 2015). It is a Pearson correlation coefficient (Pearson, 1895) calculated from comparing the intensities of equivalents by randomly dividing them into two subsets, each containing a half. Since there is a lack of a generally applicable threshold, different values of CC1/2 have been suggested. In addition, when multiplicity is odd, this division excludes a set of reflections, leading to a CC1/2 evaluated with only a portion of the data. This partiality may not be an issue as it is the average for a resolution shell but could affect its estimation at high resolution shells when the in-shell multiplicity dramatically decreases as fewer reflections become measurable.

It is worth pointing out that, in addition to decay, there exist systematic errors from various sources in a diffraction experiment which can't be cancelled out through merging. Some of them can be reduced through system calibration, whereas others may arise within the experiment such as radiation damage, crystal centering etc. The σI(*i*) is evaluated through error models during scaling

(Hamilton et al., 1965; Otwinowski et al., 1997; Kabsch, 2010; Leslie et al., 2007; Evans et al., 2013; Fu, 2005; Winter et al., 2018; Giacovazzo, 1992). Therefore, while the quality of a reduced data set typically improves as *Multi* increases, the magnitude of such improvement is conditional and can only be evaluated on a case by case basis. Details on how data quality improves with *Multi* in different cases is not the subject of this study.

Rmerg, Rmeas, Rpim derived from the minimization process of target function (1) are direct indicators of the differences among intensities of equivalent reflections. CC1/2 is also calculated from comparing the intensities of the equivalents, but in a different form. Pearson statistics (Pearson, 1895; Boslaugh, 2012) are widely used to quantitatively describe the relationships among different variables, for example how one variable tracks the changes of another variable. They could provide a tool to shed light on the relationships, the effectiveness, and capabilities of these indicators, and may help identify the most reliable metrics to evaluate and select the best data set for structure solution. Pearson Correlation Coefficient (denotated as pcc hereafter) is a coefficient that measures linear correlation between two variables, U and W. It is a normalized ratio between the covariance of two variables and the product of their standard deviations, ranging between -1 and 1 inclusive. Its sign is determined by the regression slope: positive implies that W increases while U increases; negative means W increases as U decreases. The absolute value |pcc| measures how closely the two variables correlate. A value of 1 implies a perfect dependency, while 0 indicates that there is no dependency.

I/σI, Rmerg, Rmeas, Rpim, and CC1/2 are evaluated in different resolution shells at the end of data processing. Each of them can be treated as a variable with the values indexed by resolution shell, and a pcc between each pair (U, W) of these measures can be calculated by,

$$\text{pcc}(U,W)=\frac{cov(U,W)}{\sigma U \cdot \sigma W} \quad (4).$$

Here *cov(U,W)* is the covariance of U, W. σU, σW are the standard deviations of U and W respectively.

Test and Results

1. How does CC1/2 correlate to I/σI?

To answer this question, we surveyed 815 data sets recently collected for a variety of projects by different research groups, with low-shell Rmerg better than 0.080 (to reduce disturbance from possible mis-indexing (Evans et al., 2013)), CC1/2 above 0.0 and resolution better than 6.0Å. All data sets were processed by XDS (Kabsch, 2010) and AIMLESS (Evans, 2011) (see Supplementary 1 for the detailed statistics). The plot of CC1/2 vs I/σI in the highest-resolution-shell (Figure 1A) shows a wide distribution, which suggests that CC1/2 does not have a close correlation with I/σI. This seems quite contradictory to the results described earlier that is based on assumed models (Karplus et al., 2015). For example, the high-resolution-shell I/σI ranges from 0.1 to 2.8 for those 478 data sets with CC1/2 between 0.1 and 0.4. Figure 1B shows the breakdown of the number of these data sets vs I/σI. A majority (84%) of them have I/σI below 1.1, and 69% have an I/σI below 0.9. The overall *Multi* likewise covers a large range of [1.1, 32.7], with a median at 10.1 and an average of 10.4. The CC1/2's low correlation to I/σI in the high-resolution shell seems intrinsic, and is not attributable to *Multi*. For strong reflections, when *Multi* increases, the I/σI could improve by a factor up to $\sqrt{Multi}$ as merging cancels out the random errors while

systematic errors are negligible. However, as the reflection intensity decreases, systematic errors will become more and more significant compared to the intensity, the magnitude of improvement will get less than $\sqrt{Multi}$. In the high-resolution shells, the *Multi* will also be significantly smaller than the overall as fewer reflections become measurable. Therefore, using the *Multi*, especially the overall *Multi*, to describe I/σI's dependency within the high-resolution shell is conceptually inappropriate. It's also worth pointing out that 64 of the 815 data sets were detected by AIMLESS to exhibit noticeable anisotropy with ANSdd bigger than 5%, and in one very severe case, with an ANSdd value of 37.4%. ANSdd denotes the max{2.0(r*i* – r*j*)/(r*i* + r*j*) | *i*,*j*=1,2,3; r*i* is the estimated resolution along d*i*} hereafter for simplicity.

Figure 1A. Plot of high-resolution-shell CC1/2 vs high-resolution-shell I/σI of the 815 data sets.

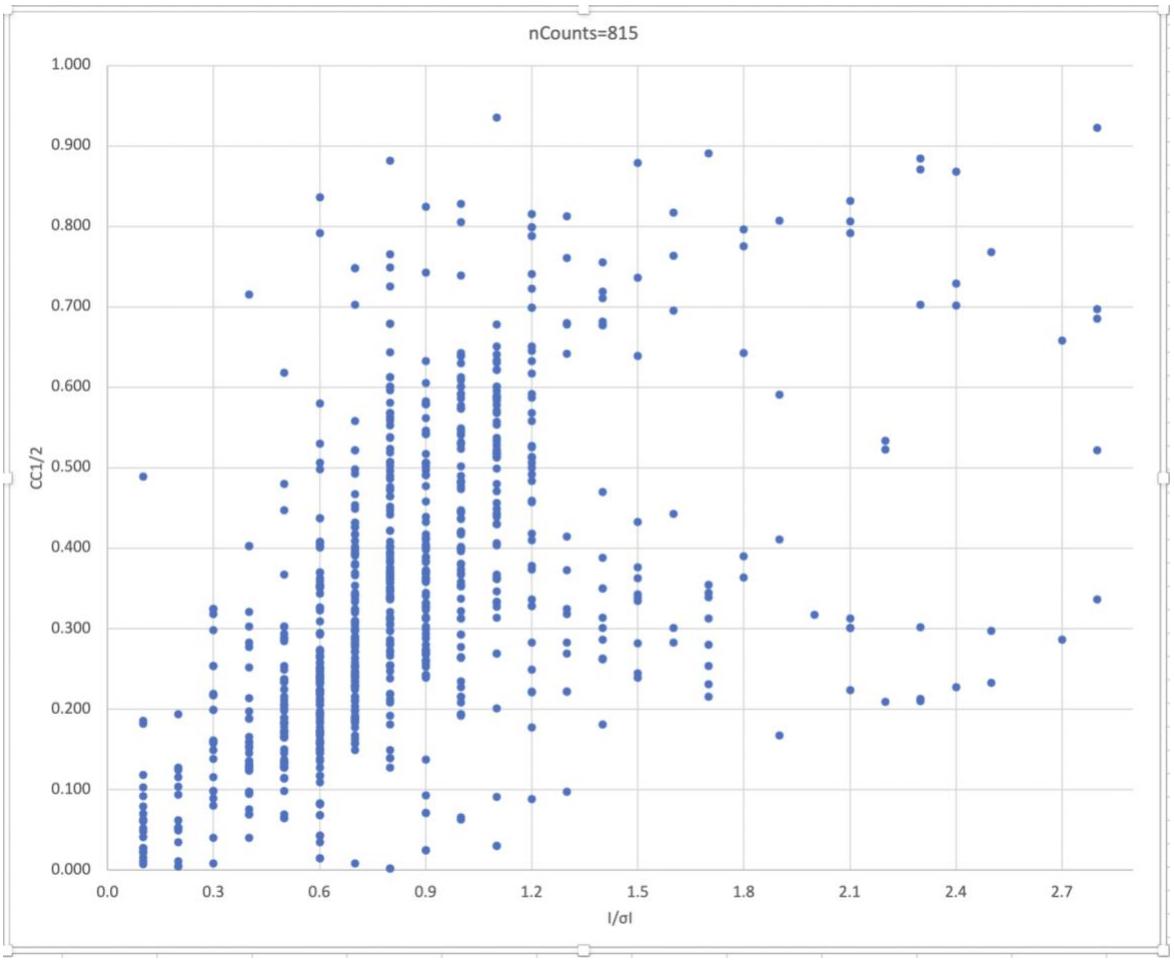

Figure 1B. Breakdown of number with I/σI out of the 478 data sets with high-resolution-shell CC1/2 in the range [0.1, 0.4].

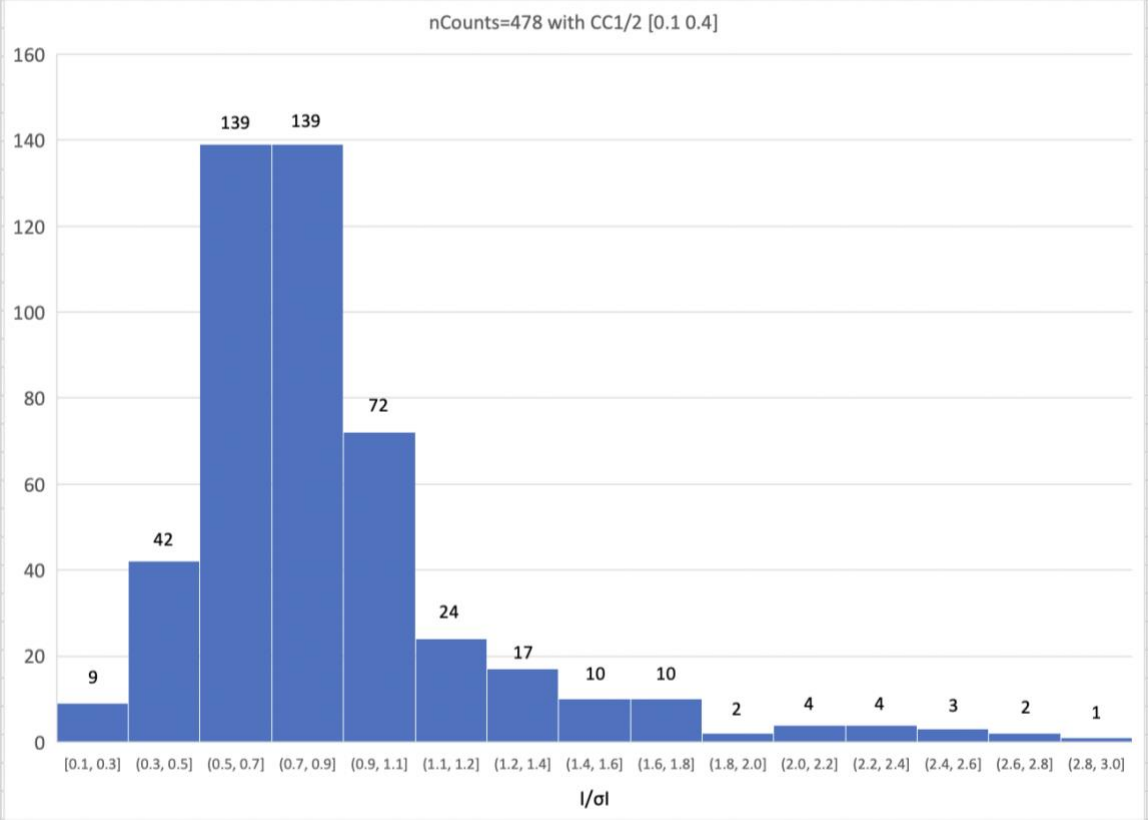

2. How are Rmerg, Rmeas, Rpim, CC1/2 correlated to each other?

As mentioned in the Methods section, Rmerg, Rmeas, Rpim and CC1/2 are all derived from comparing the intensities of equivalent reflections. To understand how these metrics are correlated, pcc values (see equation 4) among them were evaluated using experimental data with various characteristics (see Table 1). The trypA data set was collected from one standard crystal of bovine trypsin (223 amino acid residues) of P212121 symmetry by one sweep of 120º. The trypB data set was collected from a separate bovine trypsin crystal with one 720° sweep but was processed into two different reduced sets using the first 30° and all 720° of data (denoted as trypB30 and trypB720 hereafter) respectively. Data6OPM, Data7MRQ, Data8D7K and Data9ATU are data for solving the structures deposited in PDB with corresponding IDs. Data ANSdd125, ANSdd227, ANSdd313 and ANSdd374 are 4 of those 64 data sets (described in section 1) with anisotropic ANSdd of

12.5%, 22.7%, 31.3% and 37.4% respectively. MERG10 is merged from 10 data sets each from a different bovine trypsin crystal with a 20º sweep. trypA, trypB, Data8D7K, ANSdt125,227,313,374 were all indexed and integrated with XDS and scaled by AIMLESS. Data6OPM were indexed and integrated with XDS and scaled with XSCALE (Kabsch, 2010). Data7MRQ and Data9ATU were processed with HKL2000 (Otwinowski et al., 1997). MERG10 were indexed and integrated with DIALS (Winter et al., 2018) and merged by XIA2.MULTIPLEX (Gildea et al., 2022). trypADLS is trypA processed by DIALS. Values of all the measures by resolution shell were harvested from data processing (see Supplementary 2 for details). trypB30 with *Compl* 50% and *Multi* of 2 is used to evaluate pcc for incomplete data. All other data are complete with *Compl* above 90% and *Multi* between 3 to 26.

Table 1. The pcc calculated using equation 4 among Rmerg, Rmeas, Rpim and CC1/2: MgMs=pcc(Rmerg,Rmeas), MgPm=pcc(Rmerg,Rpim), MsPm=pcc(Rmeas,Rpim), MgCc=pcc(Rmerg,CC1/2), MsCc=pcc(Rmeas,CC1/2), PmCc=pcc(Rpim,CC1/2).

pcc	MgMs	MgPm	MsPm	MgCc	MsCc	PmCc
trypA	0.998	0.988	0.996	-0.979	-0.979	-0.971
trypADLS	1.000	0.999	0.999	-0.984	-0.984	-0.984
trypB30	1.000	1.000	1.000	-0.918	-0.916	-0.918
trypB720	1.000	0.986	0.989	-0.892	-0.900	-0.951
Data6OPM	1.000	1.000	1.000	-0.959	-0.959	-0.958
Data7MRQ	1.000	0.994	0.996	-0.959	-0.964	-0.978
Data8D7K	1.000	1.000	1.000	-0.984	-0.984	-0.984
Data9ATU	1.000	0.989	0.992	-0.956	-0.960	-0.972
ANSdt125	0.999	0.995	0.998	-0.939	-0.950	-0.967
ANSdt227	1.000	0.999	1.000	-0.967	-0.971	-0.976
ANSdt313	1.000	1.000	1.000	-0.992	-0.992	-0.992
ANSdt374	1.000	1.000	1.000	-0.900	-0.902	-0.903
MERG10	0.999	0.972	0.982	-0.914	-0.904	-0.982

Table 1 shows that Rmerg, Rmeas and Rpim are highly correlated with pcc approaching the perfect value 1.0. This really does not provide any new information as they are related by defined formulas and the pcc are supposed to be 1.0 theoretically. Surprisingly, |pcc| between CC1/2 and Rmerg,

Rmeas or Rpim are also very high, which suggests that CC1/2 is also highly correlated with Rmerg, Rmeas and Rpim. The negative sign only means CC1/2 decreases while the other three increase.

3. Correlations of Rmerg, Rmeas, Rpim, CC1/2, and I/σI with Resolution

Rmerg, Rmeas, Rpim, CC1/2 and I/σI have all been used to select resolution cutoffs. To compare how these indicators track resolution changes, their pcc with resolution were calculated for the 13 data sets listed in Table 1, and the results are summarized in Table 2. From Table 2, all these pcc can be different for different data sets. But for the same data set, the pcc of Rmerg, Rmeas and Rpim with resolution are very close or almost the same. The pcc of CC1/2 are either close to or smaller than those of Rmerg, Rmeas and Rpim for 12 out of the 13 data sets tested, and only larger but still comparable for data ANSdd374 which shows severe anisotropy. This suggests that CC1/2 is even less sensitive than Rmerg, Rmeas or Rpim as an indicator for selecting resolution cutoffs, which explains why CC1/2 does not have a generally applicable threshold for different cases, similar to Rmerg, Rmeas and Rpim. More interestingly, the pcc between I/σI and resolution are significantly greater than those of Rmerg, Rmeas, Rpim and CC1/2 across all 13 data sets. This suggests that I/σI values track the resolution changes more closely, which can be theoretically explained by the Debye-Waller theory (Debye, 1913; Waller, 1923). Reflection intensity decreases as the diffraction angle increases due to attenuation by atomic dynamics. Defects of the crystal could also contribute to observed attenuation. In other words, intensity I(i) and thus signal-to-noise ratio I/σI will decrease with resolution. This provides an obvious way to judge data significance from the average signal-to-noise ratio of the merged intensities as a function of resolution (Evans et al., 2013). Therefore, I/σI is much more sensitive as an indicator to select resolution cutoffs than other metrics.

Table 2. The pcc calculated using equation 4 between Rmerg, Rmeas, Rpim, CC1/2, I/σI and resolution.

pcc	Rmerg	Rmeas	Rpim	CC1/2	I/σI
trypA	-0.552	-0.535	-0.508	0.535	0.876
trypADLS	-0.842	-0.841	-0.838	0.767	0.997
trypB30	-0.605	-0.601	-0.605	0.482	0.824
trypB720	-0.560	-0.553	-0.503	0.367	0.774
Data6OPM	-0.469	-0.469	-0.466	0.349	0.888
Data7MRQ	-0.686	-0.678	-0.643	0.541	0.879
Data8D7K	-0.467	-0.468	-0.470	0.510	0.853
Data9ATU	-0.771	-0.765	-0.718	0.626	0.904
ANSdd125	-0.455	-0.447	-0.431	0.318	0.761
ANSdd227	-0.541	-0.548	-0.559	0.569	0.800
ANSdd313	-0.486	-0.486	-0.485	0.439	0.773
ANSdd374	-0.559	-0.560	-0.561	0.677	0.865
MERG10	-0.868	-0.857	-0.796	0.710	0.986

4. What do Rmerg, Rmeas, Rpim, CC1/2, and I/σI really measure? How to use them?

The high correlations among Rmerg, Rmeas, Rpim, and CC1/2 and their similar correlations across resolution point to the fact that these metrics are all derived from comparing intensities of equivalent reflections (including both Laue-symmetry-related and repeated measurements of same **H**, see Methods), although CC1/2 takes a different formula. The underlying fundamental of these indicators is Laue-symmetry. Therefore, what they measure is the same, namely the equivalency or internal consistency among reflections (Evans et al., 2013)). As the equivalents include not only the repeated measurements of the same **H** but also those that are Laue-symmetry-related, they also represent the precision of a reduced data set to certain extent. Therefore, it may be inappropriate or debatable to differentiate CC1/2 from {Rmerg, Rmeas and Rpim} by saying that CC1/2 assesses the precision of the merged data while others do not (Karplus et al., 2015; Diederichs, 2015). In a contemporary diffraction experiment with an area detector, a majority of reflections are symmetry-

related, and thus Rmerg (as its previous name Rsym suggested), Rmeas, Rpim and CC1/2 in the low-resolution-shell can serve as a reliable indicator for the correctness (or trueness) of symmetry.

I/σI, defined as SNR (signal-to-noise ratio), behaves quite differently as demonstrated above. Since I/σI is derived from merging all the equivalents, it carries partial information of both precision and accuracy. It is the only indicator directly measuring the signal strength compared with estimated error. In addition, it has the highest correlation with resolution, with both the Debye-Waller theory and Laue-symmetry as the underlying fundamentals. Therefore, compared with the group of {Rmerg, Rmeas, Rpim, CC1/2}, I/σI is arguably the most sensitive and most reliable indicator to select a resolution cutoff. Furthermore, the overall I/σI is also meaningful indicating the overall strength of a data set. This can be very helpful to compare different data sets.

5. Resolution extension beyond I/σI of 2.0

I/σI is commonly used with a threshold of 2.0 to select a resolution cutoff. The research papers with the introduction of CC1/2 (Karplus et al., 2012; Karplus et al., 2015) had a great contribution to the field by demonstrating that resolution cutoffs selected by traditional thresholds of I/σI and/or Rmerg, Rmeas, and Rpim may be too conservative for some cases. Nevertheless, due to the lack of a generally applicable threshold, the resolutions extended by some to somewhat arbitrary CC1/2 values (say 0.1, 0.2, 0.3, 0.4 etc.) need to be validated through further analysis (Evans et al., 2013; Karplus et al., 2015; Maly, et al., 2020). To understand the model improvements enabled by using weak data, we studied three cases as examples. The first one is bovine trypsin. Data trypA (processed to 1.14Å, described in section 2) of resolution 1.53Å, where {I/σI=2.0, CC1/2=0.786}, was used to solve the structure by molecular replacement with PHASER (McCoy et al., 2007)

inside PHENIX package (Liebschner et al., 2019). The model was completed with COOT (Emsley et al., 2010) and refined with PHENIX.REFINE (Afonine et al., 2012). The second is the NE/Eap4/NE complex with 6 chains of two different proteins, whose structure was originally solved at 2.05Å (PDB ID 9ATU) (Mishra et al., 2024). The third is a fragment of chicken CNTN4 that includes four point mutations in its binding site for amyloid precursor protein originally solved at 3.20Å (PDB ID 7MRQ) (Karuppan et al., 2021). Step-by-step paired-refinements following the published protocols (Karplus et al., 2015; Maly, et al., 2020; Winter et al., 2018) were carried out to extend to higher resolution (see Table 3). PHENIX.REFINE was used for each refinement. As shown in equation (3), the electron density map is the Fourier transform of all reflections to a selected resolution. Its quality depends collectively not only on the overall quality of all the reflections, but also on both the geometry and B-factors of all atoms, and *vice versa*. For the trypsin and NE/Eap4/NE cases, the resolutions to be checked were all within the range where auto-tracing works well. Instead of directly comparing the R/Rfree/Rgap (Rgap is the difference of Rfree and R) from refinements, we slightly modified the protocol by auto-tracing the refined electron density maps from each refinement with PHENIX.AUTOBUILD (Terwilliger et al., 2008) and compared the resulting R/Rfree/Rgap, which would add a quantitative evaluation of the qualities of electron density maps.

Table 3. Paired-Refinements to verify extended resolutions. (A). Tryspin; (B). NE/Eap4/NE; (C). CNTN4. The data used are 'trypA', 'Data9ATU', and 'Data7MRQ' respectively (see section 2 and Supplementary 2 for details of reduction statistics). Here, R.I.C. is the target with {Resolution, in-shell I/σI, in-shell CC1/2} to check, which will also serve as the reference of next step; R.L.={R, Rfree at lower or reference resolution}, RH={R, Rfree at higher or target resolution to check}. The test is considered true if two of {R, Rfree, Rga} are better or Rfree is close and Rgap is better.

Table 3(A).

Trial	R.I.C.	R.L.	R.H.	Test
start	{1.53 2.0 0.786}	{------ ------}	{------ ------}	----
step1	{1.44 1.3 0.722}	{0.1984 0.2234}	{0.2020 0.2273}	true
step2	{1.40 1.1 0.657}	{0.2051 0.2282}	{0.2038 0.2262}	true
step3	{1.34 0.8 0.591}	{0.2061 0.2241}	{0.2036 0.2211}	true
step4	{1.25 0.5 0.464}	{0.2157 0.2311}	{0.2285 0.2448}	false

Table 3(B).

Trial	R.I.C.	R.L.	R.H.	Test
start	{2.10 2.2 0.757}	{------ ------}	{------ ------}	----
step1	{2.03 1.4 0.476}	{0.2205 0.2545}	{0.2167 0.2488}	true
step2	{1.95 0.7 0.275}	{0.2210 0.2596}	{0.2245 0.2680}	false

Table 3(C).

Trial	R.I.C.	R.L.	R.H.	Test
start	{3.18 2.0 0.843}	{------ ------}	{------ ------}	----
step1	{3.10 1.5 0.853}	{0.2026 0.2309}	{0.2052 0.2310}	true
step2	{3.04 1.2 0.702}	{0.1994 0.2308}	{0.2071 0.2226}	true
step3	{2.98 0.9 0.491}	{0.1985 0.2249}	{0.2022 0.2272}	true
step4	{2.92 0.7 0.304}	{0.2014 0.2396}	{0.2021 0.2447}	false

For trypsin data, 1.53Å is selected by a traditional I/σI=2.0 cutoff. The paired-refinements demonstrated that the resolution could be extended to 1.34Å (a gain of 0.19Å). This agrees well with the Wilson plot in Figure 2(A), which starts to deviate around 1.4Å and clearly gets abnormal or suspicious beyond resolution of 1.3Å. From curiosity on how noisy or weak data would affect the electron density map, we refined the model using all the data up to 1.14 Å at which CC1/2=0.202 and I/σI=0.1, followed by a PHENIX.AUTOBUILD. If the contribution from the noisy data in the high-resolution shell is positive, a better electron density map and thus a better traced model would be expected. But the result shows otherwise. Figure 2(B) is part of the electron density maps around SER119 superposed with the traced models from using resolutions 1.14Å (left) and 1.40Å (Right), respectively. The electron density map from 1.14Å cutoff looks significantly noisier. For example, its auto-tracing failed building GLY120 after SER119 due to

too much erroneous extra density, leading to one of 2 main-chain gaps. The erroneous density also affected the building of side chains (such as a TYR was built instead of the correct TRP121).

Figure 2. (A) Wilson plot calculated by WILSON in CCP4 (Winn et al., 2011) of trypA, where d is resolution. (B) part of the electron density maps around SER119 superposed with the traced models from PHENIX.AUTOBUILD for resolution cutoff of 1.14Å (Left) and 1.40Å (Right), respectively, displayed by COOT defaults.

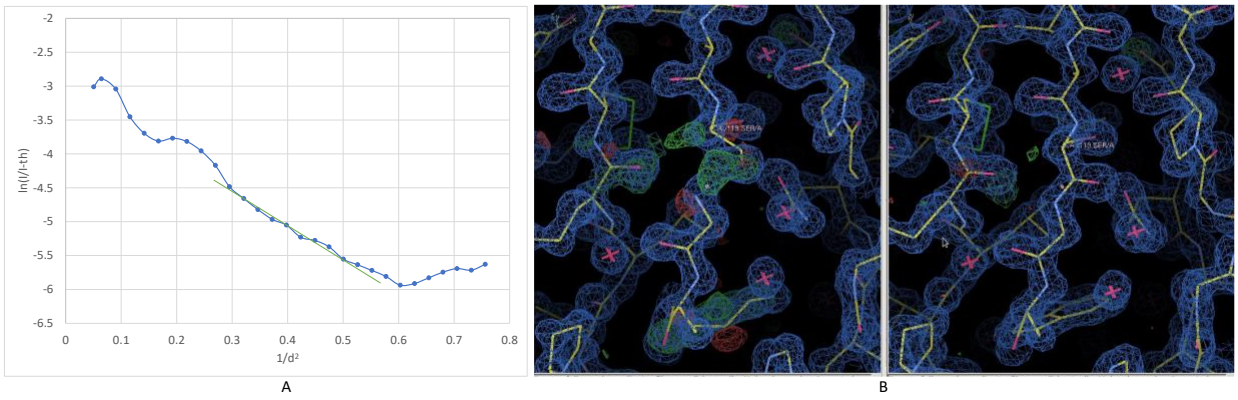

For the NE/Eap4/NE data, we took the deposited structure in the PDB and refined at 2.10Å as the starting model. The resolution could be extended to 2.03Å by paired-refinement verification (a gain of 0.07Å). For the CNTN4 data, the PDB deposition was first refined at 3.18Å and then served as the starting model. The resolution could be extended to 2.98Å through paired-refinements (a gain of 0.20Å). Figure 3 shows that the Wilson plots start to deviate around 2.0Å and 3.0Å for NE/Eap4/NE and CNTN4 data, respectively.

Figure 3. Wilson plot calculated with WILSON in CCP4. (A) NE/Eap4/NE data. (B) CNTN4 data.

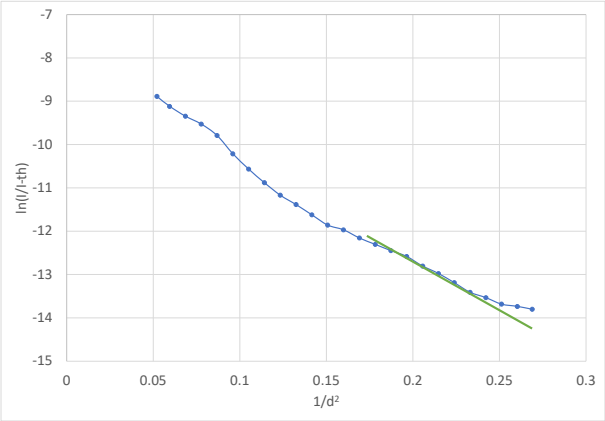

Fig 3(A)

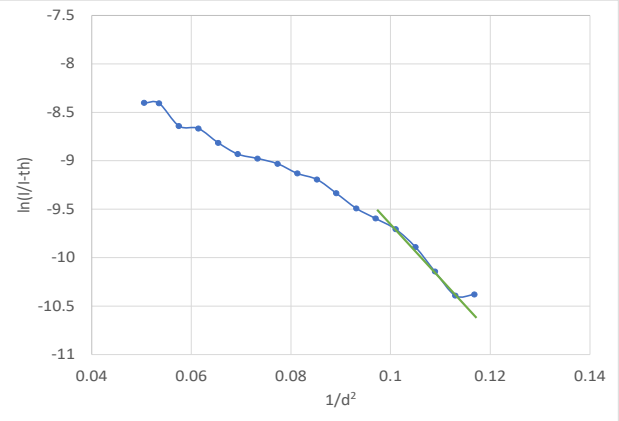

Fig 3(B)

It's worth noticing that, since both I/σI and CC1/2 drop suddenly and quickly at high-resolution shells beyond the resolution cutoffs selected by a traditional I/σI $\geq$ 2.0, the extensions are typically limited (Evans et al., 2013; Karplus et al., 2015; Maly, et al., 2020; Winter et al., 2018). This may look small but could be more significant in low-resolution or challenging cases.

As expected, when noisier data were gradually added by extending to higher resolution, the overall R/Rfree became worse. It makes sense for 'paired-refinement' to compare the R/Rfree at the same and lower resolution. However, all the data to the extended resolution cutoff must be used to evaluate the final model quality and R/Rfree. Table 4 lists statistics from the final refinements using all reflections to the different resolutions selected, which shows that adding the noisy and weak data in the extended higher resolution shell didn't change the geometry of the model or did so in a very limited fashion. On the other hand, the B-factors (both the average representing the overall and the minimum indicating the bottom-line) all became noticeably worse, which would suggest an overall deterioration or no improvement of electron density quality.

Table 4. Final refinements using all data to the extended resolutions tried. (A). Trypsin; (B). NE/Eap4/NE; (C). CNTN4. R/Rfree is the overall from final refinements. <B>(min) is the average and the minimum B-factors. RMSD is from the pair-wise 3D-structure alignment of the models using USALIGN (Zhang et al., 2022).

Table 4(A).

Reso	R/Rfree		<B>(min)	RMSD{models(A,B)}		
1.53	0.1766	0.1953	11.8(5.8)	----		
1.44	0.1871	0.2098	12.0(6.1)	0.02	----	
1.40	0.1901	0.2031	13.0(6.7)	0.02	0.02	----
1.34	0.1963	0.2158	13.1(7.4)	0.02	0.02	0.01

Table 4(B).

Reso	R/Rfree		<B>(min)	RMSD{models(A,B)}
2.10	0.1802	0.2148	58.9(30.4)	----
2.03	0.1833	0.2235	60.8(32.3)	0.03

Table 4(C).

Reso	R/Rfree		<B>(min)	RMSD{models(A,B)}		
3.18	0.2041	0.2306	86.6(51.6)	----		
3.10	0.2065	0.2313	93.3(54.5)	0.06	----	
3.04	0.2079	0.2335	95.5(55.8)	0.07	0.07	----
2.98	0.2183	0.2409	89.3(57.6)	0.06	0.06	0.06

6. Be careful of both geometry and B-factor changes when trying to extend resolution cutoffs

The most critical factors that determine structure quality include resolution, quality of the electron density map, model geometry, B-factors and R/Rfree. A valid resolution cutoff extension should be, at least: (1) the electron density shows structural features that match the resolution, fewer or no change of disordered regions, and gets cleaner with less erroneous extra density; (2). better or no change in Ramachandran plot and Clashscore (as modern refinement programs usually do not allow large deviations of bond lengths and angles from ideal values, Ramachandran plot and Clashscore may not show much difference during paired-refinements); (3). smaller or no significant increase of B-factors which may not be a proof of no deterioration of electron density quality, but a dramatic increase will be a sign of deterioration; (4). better or no significant increase in R/Rfree.

As shown in equation 3, changing B-factors have a large impact on the electron density. It is well known that after the molecules are correctly built, B-factors become the most efficient means of reducing R/Rfree during the refinement, thus R/Rfree alone is not able to fully access the structure's quality. However, aggressively extending the resolution to a higher cutoff would likely make the quality worse if the geometry doesn't change much but B-factors are pushed significantly higher to account for the errors. Indeed, out of the latest 100,000 structures in PDB solved by X-ray diffraction, the average B-factor of macro molecules in the 14,283 structures with reported high-shell I/σI between 1.0 and 2.0 is 49.9, while the average B-factor of all the 4,326 structures with reported high-shell I/σI below 1.0 is significantly worse at 59.4.

7. About I/σI from Different Data Processing Programs

It was reported (Karplus et al., 2015) that different data processing programs may have different evaluated values of I/σI. We processed the trypA with different programs (see Table 5). Table 5 didn't show more differences in I/σI than CC1/2, except DIALS, which came into use recently compared to others. It's not clear why the I/σI from DIALS is significantly different from others. Although it evaluates I/σI differently (see Supplementary2 trypADLS), all the correlations (see Table 1 and Table 2) agree well with those described above. <I/σI> and <I>/<σI> can be different if σI(*i*) are significantly different among the reflections summed within a resolution shell. HKL2000 does not list <I/σI> in its output log file, but instead <I>, <σI> separately, which may be changed in its future release.

Table 5. High-resolution-shell I/σI, and CC1/2 from trypA processed by different data processing programs. IMOSFLM (Leslie et al., 2007) in the CCP4 package automatically cut the resolution

to 1.28Å. To compare apples to apples, we applied the same resolution cutoffs for DIALS, XDS (XSCALE scaling), and AIMLESS (XDS integration + AIMLESS scaling). HKL2000 didn't integrate the data beyond 1.54Å, at which the high-resolution-shell <I>, <σI> were evaluated to be 0.2, 0.3 respectively, leading to <I>/<σI>=0.67.

Program	Resolution	I/σI	CC1/2
IMOSFLM	1.28	0.7	0.304
XDS/XSCALE	1.28	0.6	0.526
XDS/AIMLESS	1.28	0.5	0.464
DIALS	1.28	1.3	0.559
HKL2000	1.54	0.7	0.566

8. Summary

Based on theoretical and pcc analysis, {Rmerg, Rmeas, Rpim, or CC1/2} all measure the equivalence of reflections, and the low-shell values of these metrics are reliable indicators for correctness (or trueness) of symmetry. Once symmetry correctness is determined, high-shell I/σI may still be the best indicator as traditionally used to select resolution cutoffs for the following reasons: 1) I/σI is the indicator that measures the signal strength compared with error levels in the data; 2) It has significantly higher correlation with resolution thus better sensitivity as an indicator; 3). The overall I/σI provides a measure of overall strength of the data, while neither that of Rmerg, Rmeas, Rpim or CC1/2 does.

Extended resolution cutoffs selected by the currently used CC1/2 values {say 0.1, 0.2, 0.3 etc.} may need further verification. Directly comparing the statistics from refinements using different resolutions plus visually checking the quality of electron density map is an obvious and straightforward way for the verification, which is traditionally and commonly used to test resolution cutoffs at the last stage of the structure solution process. The paired-refinement protocol

provides a way, less strict but maybe useful, for this purpose (Karplus et al., 2015; Maly, et al., 2020; Evans et al., 2013; Winter et al., 2018). When the extended resolutions are within the range where auto-tracing works well, using the statistics from auto-tracing of the refined models may be more convincing because: 1) Auto-tracing quantitively evaluates the overall quality of the whole electron density map; 2) R/Rfree/Rgap from the refinements alone cannot fully assess the quality of electron density. Structures solved from data with traditional resolution cutoffs selected by I/σI of 2.0 have been demonstrated to be reliable and serve as the starting models when resolution extensions are to be tried. Otherwise, a resolution cutoff corresponding to a lower I/σI of ~1.5 may represent a better starting point to save time from trial-and-errors in the whole process of structural solution.

Discussion

The quality of the final structural model from X-ray crystallography relies on the quality of the data selected at the data acquisition step. In principle, this selection could be delayed to the stage of structural refinement for a final evaluation by electron density map quality, geometry, B-factors, R/Rfree etc. However, practically speaking, structure solution still requires significant time to get to the final stage, while data acquisition is comparatively rapid. In most cases, to get the best reduced data, you may need data quality evaluation to make changes or modifications of parameters at data collection, especially transmission and more importantly detector distance that is critical for optimizing the "spot-separations (spatial resolution)" while realizing the samples' diffraction capability, which in turn will affect the background and errors estimation in data processing and thus the quality of the reduced data. Rmerg, Rmeas, Rpim and CC1/2 have been used to measure data quality and select resolution cutoffs, but none of them seems as sensitive,

meaningful, or accurate as I/σI. More importantly, compared to I/σI, each of them lacks a generally applicable threshold for different cases.

Nowadays, most structures are solved by using existing structures as templates through molecular replacement or docking into Cryo-EM maps. In the long run, it will be beneficial for X-ray crystallography to keep producing more high-quality structures by holding up its data selection standards. Furthermore, prediction accuracy will be improved when more high-quality structures are available for AI-based modeling programs such as AlphaFold (Jumper et al., 2021; Abramson et al., 2024), RoseTTAfold (Baek et al., 2021) etc. to train their models. It is worth pointing out that crystal diffraction methods refine the B-factor in addition to the position for each atom in the structure model. High-quality structures will have lower errors in B-factors, and thus, will be more suitable for studying molecular dynamics (Ringe et al., 1986; Carugo et al., 1997; Winn et al., 2001; Sun et al., 2019; Pearce et al., 2021) or for quantifying and detecting radiation damage (Kathryn et al., 2022). That said, it would be beneficial for journals and grant reviewers to add some credit to researchers that report structures already solved but repeated with significantly higher quality. It would also be beneficial to include the key data selection standard in both publications and PDB depositions, which would provide a tracking record for quick reference in the future.

Acknowledgement

This research is funded and supported by the Southeast Regional Collaborative Access Team (SER-CAT) Member Institutions (a list may be found on the SER-CAT website), the University of Georgia Research Foundation, and the Georgia Research Alliance, and is also supported in part

by grant R35GM140852 to BVG and by award number R15NS108371 to SB. We thank Dr. Yifan Cheng of HHMI & University of California San Francisco for discussion on the current developments of Cryo-EM. We also thank Dr. Stephen K. Burley, Director of the RCSB Protein Data Bank for critically reviewing the manuscript and providing feedback. X-ray diffraction data were collected at SER-CAT beamline 22-ID at the Advanced Photon Source, Argonne National Laboratory. Use of the Advanced Photon Source was supported by the U.S. Department of Energy, Office of Science, Office of Basic Energy Sciences, under Contract No. W-31-109-Eng-38.

Author Contributions

ZQF conceived the project and performed the analysis. ZQF and BVG prepared the draft. BVG, SB and FD assisted in the analysis. JC organized the beamline for data collection. PK checked and formatted the References. PK, DJM, BCW helped in works related to structural biology. All coauthors participated in critical reading of the paper.

Data Availability Statement

All data generated or analyzed during the study are included in this published article and its supplementary information files.

References

Abramson, J., Adler, J., Dunger, J., Evans, R., Green, T., Pritzel, A., Ronneberger, O., Willmore, L., Andrew J., Ballard, A.J., Bambrick, J., Bodenstein, S.W., Evans, D. A., Hung, C., O'Neill, M., Reiman, D., Tunyasuvunakool, K., Wu, Z., Žemgulytė, A., Arvaniti, E., Beattie, C., Bertolli, O., Bridgland, A., Cherepanov, A., Congreve, M., Cowen-Rivers, A.I., Cowie, A., Figurnov, M., Fuchs, F.B., Gladman, H., Jain, R., Khan, Y.A., Low, C.M.R., Perlin, K., Potapenko, A., Savy, P., Singh, S., Stecula, A., Thillaisundaram, A., Tong, C., Yakneen, S., Zhong, E.D., Zielinski, M., Žídek, A., Bapst, V., Kohli, P., Jaderberg, M., Hassabis, D. & Jumper, J.M. (2024). *Nature*. **630**, 493-500.

Afonine, P.V., Grosse-Kunstleve, R.W., Echols, N., Headd, J.J., Moriarty, N.W., Mustyakimov, M., Terwilliger, T.C., Urzhumtsev, A., Zwart, P.H. & Adams, P.D. (2012). *Acta Cryst*. **D68**, 352-367.

Agirre, J., Atanasova, M., Bagdonas, H., Ballard, C.B., Basle´, A., Beilsten-Edmands, J., Borges, R.F., Brown, D.G., Burgos-Marrmol, J.J., Berrisford, J.M., Bond, P.S., Caballero, I., Catapano, L., Chojnowski, G., Cook, A.G., Cowtan, K.D., Croll, T.I., Debreczeni, J.E., Devenish, N.E., Dodson, E.J, Drevon, T.R., Emsley, P., Evans, G., Evans, P.R., Fando, M., Foadi, J., Fuentes-Montero, L., Garman, E.F., Gerstel, M., Gildea, R.J. Hatti, K., Hekkelman, M.L., Heuser, P.,Hoh, S.W., Hough, M.A., Jenkins, H.T., Jime´nez, E., Joosten, R.P., Keegan, R.M., Keep, N., Krissinel, E.B., Kolenko, P., Kovalevskiy, O., Lamzin, V.S., Lawson, D.M., Lebedev, A.A., Leslie, A.G.W., Lohkamp, B., Long, F., Maly, M., McCoy, A.J., McNicholas, S.J., Medina, A., Milla´n, C., Murray, J.W., Murshudov, G.N., Nicholls, R.A.,Noble, M.E.M., Oeffner, R., Pannu, N.S., Parkhurst, J.M., Pearce, N., Pereira, J., Perrakis, A., Powell, H.R., Read, R.J., Rigden, D.J., Rochira, W., Sammito, M., Rodrı´guez, F.S., Sheldrick, G.M., Shelley, K.L., Simkovic, F., Simpkin, A.J., Skubak, P., Sobolev, E., Steiner, R.A., Stevenson, K., Tews, I., Thomas, J.M.H., Thorn, A., Valls, J.T., Uski, V., Uso´n, I., Vagin, A., Velankar, S., Vollmar, M., Walden, H., Waterman, D., Wilson, K.S., Winn, M.D., Winter, G.,Wojdyr, M. & Yamashita, K. (2023). *Acta Cryst.* **D79**, 449-461.

Baek, M., DiMaio, F., Anishchenko, I., Dauparas, J., Ovchinnikov, S., Lee, G.R., Wang, J., Cong, Q., Kinch, L.N., Schaeffer, D., Millán, C., Park, H., Adams, C., Glassman, C.R., DeGiovanni, A., Pereira, J.H., Rodrigues, A.V., Van Dijk, A.A., Ebrecht, A.C., Opperman, D.J., Sagmeister, T., Buhlheller, C., Pavkov-Keller, T., Rathinaswamy, M.K., Dalwadi, U., Yip, C.K., Burke, J.E., Garcia, K.C., Grishin, N.V., Adams, P.D., Read, R.J. & Baker, D. (2021). *Science*. **373**, 871-876.

Berman, H.M., Westbrook, J., Feng, Z., Gilliland, G., Bhat, T.N., Weissig, H., Shindyalov, I.N. & Bourne, P.E. (2000). *Nucleic Acids Res*. **28**, 235-242.

Berman, H.M., Henrick, K. & Nakamura, H. (2003). Nature Structural & Molecular Biology 10, 980. https://doi.org/10.1038/nsb1203-980.

Boslaugh, S. (2012). *Statistics in a Nutshell, 2nd Edition.* O'Reilly Media, Inc.

Brünger, A.T. (1992). *Nature.* **355**, 472-475.

Burley, S.K., Bhikadiya, C., Bi C., Bittrich, S., Chao, H., Chen, L., Craig, P.A., Crichlow, G.V., Dalenberg, K., Duarte, J.M., Dutta, S., Fayazi, M., Feng, Z., Flatt, J.W., Ganesan, S., Ghosh, S., Goodsell, D.S., Green, R.K., Guranovic, V., Henry, J., Hudson, B.P., Khokhriakov, I., Lawson, C.L., Liang, Y., Lowe, R., Peisach, E., Persikova, I., Piehl, D.W., Rose, Y., Sali, A., Segura, A., Sekharan, M., Shao, C., Vallat, B., Voigt, M., Webb, B., Westbrook, J.D., Whetstone, S., Young, J.Y., Zalevsky, A. & Zardecki, C. (2023). *Nucleic Acids Res*. **51**, D488-D508.

Carugo, O. & Argos, P. (1997). *Protein Eng. Des. Sel.* **10**, 777-787.

Cheng, Y., Grigorieff, N., Penczek, P.A. & Walz, T. (2015). *Cell*. **161**, 438-449.

Debye, P. (1913). *Annalen der Physik.* **348**, 49-92.

Diederichs, K. & Karplus, P.A. (1997). *Nat. Struct. Mol. Biol.* **4**, 269-275.

Diederichs,K. (2016). *Nucleic Acids Crystallography: Methods and Protocols.* **1320**. Edited by Eric Ennifar, New York: Springer.

Dubochet, J. & Knapek, E. (2018). *PLoS Biol*. **16**, e2005550.

Emsley, P., Lohkamp,b Scott, W. & Cowtan, K. (2010*). Acta Cryst*. D**66**, 486-501.

Evans, P.R. (2011). *Acta Cryst.* D**67**, 282-292.

Evans, P.R. and Murshudov, G.N. (2013). *Acta Cryst*. D**69**, 1204-1214.

Frank, J. (2009). Q Rev Biophys. **42(3)**, 139-158.

Fu, Z.-Q. (2005). *Acta Cryst.* D**61**, 1643-1648. Fu, Z.Q.: Kylin a program for crystal diffraction data reduction and data collection monitoring. (To be published).

Giacovazzo, C., Monaco, H.L., Artioli, G., Viterbo, D., Milanesio, M., Gilli, G., Gilli, P., Zanotti, G., Ferraris, G. & Catti, M. (1992). *Fundamentals of Crystallography*. Oxford University.

Gildea, R.J., Beilsten-Edmands, J., Axford, D., Horrell, S., Aller, P., Sandy, J., Sanchez-Weatherby, J., Owen, D., Lukacik, P., Strain-Damerell, C., Owen, R.L., Walsha, M.A. Winter, G. (2022). *Acta Cryst.* D**78**, 752-769.

Hamilton, W.C., Rollett, J.S. & Sparks, R.A. (1965). *Acta Cryst*. **18,** 129-130.

Henderson, R., Baldwin, J.M., Ceska, T.A., Zemlin, F., Beckmann, E. & Downing, K.H. (1990). *J. Mol. Biol*. **213**, 899-929.

Jumper, J., Evans, R., Pritzel. A., Green, T., Figurnov, M., Ronneberger, O., Tunyasuvunakoo, K., Bates, R., Žídek, A., Potapenko, A., Bridgland, A., Meyer, C., A. Kohl, S.A.A., Ballard, A.J., Cowie, A., Romera-Paredes, B., Nikolov, S., Jain, R., Adler, J., Back, T., Petersen, S., Reiman, D., Clancy, E., Zielinski, M., Steinegger, M., Pacholska, M., Berghammer, T., Bodenstein, S., Silver, D., Vinyals, O., Senior, A.W., Kavukcuoglu, K., Kohli, P. & Hassabis, D. (2021). *Nature*. **596**, 583-589.

Kabsch, W. (2010). *Acta Cryst. D***66**, 125-132.

Karplus, P.A. & Diederichs, K. (2012). *Science.* **336**, 1030-1033.

Karplus, P.A. & Diederichs, K. (2015). *Curr. Opin. Struct. Biol.* **34**, 60-68.

Karuppan,S.J., Vogt,A., Fischer,Z., Ladutska,A., Swiastyn,J., McGraw,H.F., Bouyain,S. (2021). J.BiolChem. 298: 01541.

Shelley, K.L. & Garman, E.F. (2022). *Nat. Commun.* **13**, 1314.

Leslie, A.G.W. & Powell, H.R. (2007). *NATO Science Series*, **245,** Read, R.J., Sussman, J.L. (eds) Springer, Dordrecht.

Liebschner, D., Afonine, P.V., Baker, M.L., Bunkoczi, G., Chen, V.B., Croll, T.I., Hintze, B., Hung, L. W., Jain, S., McCoy, A.J., Moriarty, N.W., Oeffner, R.D., Poon, B.K., Prisant, M.J., Read, R.J., Richardson, J.R., Richardson, D.C., Sammito, M.D., Sobolev, O.V., Stockwell, D.H., Terwilliger, T.C, Urzhumtsev, A.G., Videau, L.L., Williams, C.J & Adams, P.D. (2019). *Acta Cryst*. D**75**, 861-877.

Maly, M., Diederichs, K., Dohnalek, J. & Kolenko, P. (2020). *IUCrJ.* **7**, 681-692.

McCoy, A.J., Grosse-Kunstleve, R.W., Adams, P.D., Winn, M.D., Storoni, L.C. & Read, R.J. (2007). *J. Appl. Cryst.* **40**, 658-674.

Mishra, N., Gido, C.D., Herdendorf, T.J., Hamme, M., Hura, G.L., Fu, Z.Q. & Geisbrecht, B.V. (2024). *J. Biol. Chem*. **300**, 107627.

Murshudov, G.N., Skubak, P., Lebedev, A.A., Pannu, N.S., Steiner, R.A., Nicholls, R.A., Winn, M.D., Long, F. & Vagin, A.A. (2011). *Acta Cryst.* D**67**, 355-367.

Otwinowski, Z. & Minor, W. (1997). *Methods Enzymol.* **276**, 307-326.

Pearce, N. M. & Gros, P. (2021). *Nat. Commun*. **12**, 5493.

*Pearson, K. (1895). Proc. Royal Soc. of London. **58,** 240-242.*

Ringe, D. & Petsko, G.A. (1986). *Methods Enzymol*. **131**, 389-433.

Sun, Z., Liu, Q., Feng, Y. & Reetz, M.T. (2019). *Chem. Rev.* **119**, 1626-1665.

Terwilliger, T.C, Grosse-Kunstleve, R.W., Afonine, P.V., Moriarty, N.W., Zwart, P.H., Hung, L.-W., Read, R.J. & Adams, P.D. (2008). *Acta Cryst.* D**64**, 61-69.

Waller, I. Zur Frage der Einwirkung der Wärmebewegung auf die Interferenz von Röntgenstrahlen. (1923). *Z. Physik.* **17**, 398-408.

Weiss, M. & Hilgenfeld, R. (1997). *J. Appl. Cryst.* **30**, 203-205.

Winn, M. D., Isupov, M. N. & Murshudov, G. N. (2001). *Acta Cryst.* D**57**, 122-133.

Winn, M.D, Ballard, C.C., Cowtan, K.D., Dodson, E.J., Emsley, P., Evans, P.R., Keegan, R.M., Krissinel, E.B., Leslie, A.G.W, McCoy, A., McNicholas, S.J., Murshudov, G.N., Pannu, N.S., Potterton, E.A., Powell, H.R., Read, R.J., Vaginc, A. and Wilson, K.S. (2011). *Acta Cryst*. **D67**, 235-242.

Winter, G., Waterman, D.G., Parkhurst, J.M., Brewster, A.S., Gildea, R.J., Gerstel, M., Fuentes-Montero, L., Vollmar, M., Michels-Clark, T., Young, I.D., Sauter, N.K. & Evans, G. (2018). *Acta Cryst.* D**74**, 85-97.

Zhang,C., Shine,M., Pyle,A.M., Zhang,Y. (2022). *Nat Methods*. **19(9)**,1109-1115.